Discover Chemistry

RESEARCH Open Access

Exploring the inhibitory potential of *Lippia Javanica* phytochemicals against SARS-CoV-2 Omicron variant Mpro using molecular modelling approaches

Vincent Obakachi[1], Ayodeji Amobonye[2], Santhosh Pillai[3], Krishna Govender[1*], Penny Govender[1] and Francis O. Shode[3*]

*Correspondence:
Krishna Govender
krishnag@uj.ac.za
Francis O. Shode
franciss@dut.ac.za
[1]Department of Chemical Sciences, University of Johannesburg, Doornfontein Campus, P.O. Box 17011, Johannesburg 2028, South Africa
[2]Department of Polymer Chemistry and Technology, Kaunas University of Technology, Radvilenu Road 19, Kaunas 50254, Lithuania
[3]Department of Biotechnology and Food Science, Faculty of Applied Sciences, Durban University of Technology, P.O. Box 1334, Durban 4000, South Africa

Abstract

Amidst the emergence of SARS-CoV-2 variants and the persistence of long-term COVID-19 complications, the search for novel therapeutics remains a global priority. *Lippia javanica*, a Southern African herb traditionally used for respiratory conditions, gained prominence as a home remedy during the COVID-19 pandemic. This study represents the first in silico investigation into the inhibitory potential of 116 phytochemicals from *L. javanica*, identified through LC-MS and previous literature, against the SARS-CoV-2 Omicron variant main protease (Mpro), with nirmatrelvir serving as the reference inhibitor. Using a combination of molecular modelling approaches, physicochemical and toxicity profiling, and bioactivity prediction, five phytochemicals demonstrated competitive binding profiles relative to nirmatrelvir. Remarkably, isoverbascoside exhibited the strongest binding affinity (-9.2 kcal/mol), forming key hydrogen bonds, alkyl, π-alkyl, and van der Waals interactions. Despite a few candidates violating Lipinski's Rule of Five due to high molecular weight, they displayed favourable lipophilicity, predicted bioactivity, and low toxicity. MD simulations further confirmed the structural stability of isoverbascoside, crassifolioside, and verbascoside within the Mpro binding pocket, with binding free energies of -58.16, -48.12, and −46.54 kcal/mol, respectively, substantially surpassing that of nirmatrelvir (-34.68 kcal/mol). Stability analyses via RMSD, RMSF, and RoG metrics corroborated the dynamic integrity of these complexes. In all, the findings highlight the promising inhibitory potential of *L. javanica* phytochemicals, particularly isoverbascoside, against SARS-CoV-2 Mpro, warranting further experimental validation to confirm their therapeutic applicability.

Keywords Coronavirus therapeutics, *Lippia javanica*, Molecular modelling approaches, SARS-CoV-2 inhibitors, Main protease (Mpro)

Graphical abstract

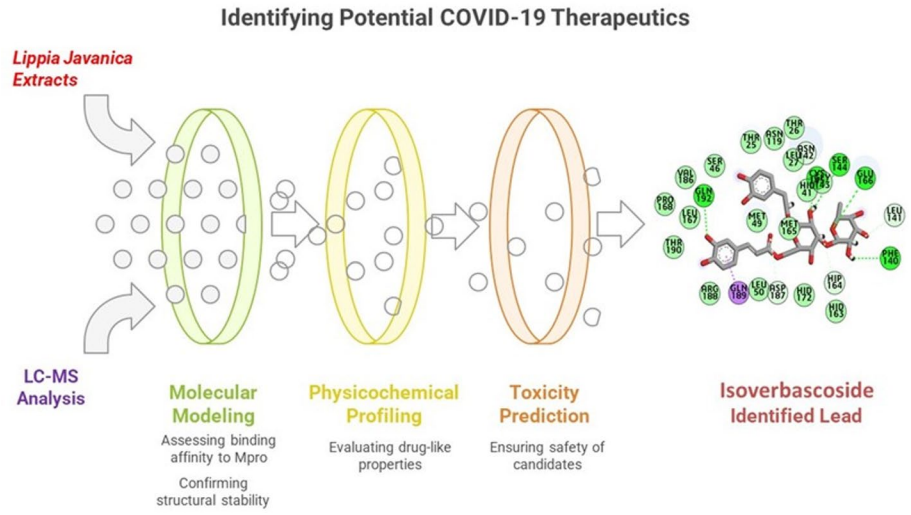

1 Introduction

Coronavirus disease (COVID-19), caused by Severe Acute Respiratory Syndrome Coronavirus 2 (SARS-CoV-2), remains one of the most devastating pandemics in modern history, characterized by significant mortality, widespread morbidity, and economic disruption [1]. As of April 2024, over 700 million confirmed cases and more than 7 million deaths were reported globally [2]. Although the World Health Organization declared the public health emergency over in May 2023, long-term complications persist among recovered patients, and socio-economic effects continue [3]. Africa, for instance, exhibited comparable infection rates to other regions but still grapples with vaccine coverage gaps and post-pandemic recovery [4]. Moreover, SARS-CoV-2 continues to evolve, with emerging variants posing renewed challenges [5].

According to Chung, et al. [6], approximately 2,000 COVID-19-related deaths were recorded between mid-May and mid-June 2024, and another wave was predicted due to the rising prevalence of Omicron subvariants. Since the identification of the original D614G variant, numerous strains have emerged, including those designated as "variants of concern" (VOCs), such as Omicron and its subvariants BA. 1 (B. 1.1.7), BA. 2, BA. 4, BA. 5, and BA. 2.12.1 (Eris) and XBB, which exhibit higher transmissibility, immune escape, and resistance to monoclonal antibodies [7–9]. While vaccines have reduced disease severity, their effectiveness has diminished against subvariants such as BA.4 and BA.5, underscoring the urgent need for alternative therapeutics [10]. Remarkably, the newer variants KP.2, KP.3, and LB.1, which are derived from JN.1, are projected to dominate upcoming infections [6].

In addition to vaccines, therapeutic drugs are essential for managing infections in high-risk populations, vaccine breakthrough cases, and immunocompromised individuals [11]. However, many drugs approved for emergency use by the US FDA have reduced efficacy against newer variants [12]. Therefore, interest has grown in small molecules, especially plant-derived compounds, as viable antiviral candidates. One strategic target is the SARS-CoV-2 main protease (Mpro/3CLpro), a crucial enzyme in the replication of the virus. Inhibiting Mpro has shown broad antiviral potential, as it is highly conserved

across all coronaviruses [13]. Currently, Mpro inhibitors are grouped into non-covalent (e.g., nirmatrelvir, remdesivir, quercetin) and covalent types (e.g., ebselen, GRL-1720, SIMR-2418) [14]. However, limitations such as drug resistance and off-target effects remain. For example, nirmatrelvir's use is constrained by potential drug-drug interactions and a lack of long-term efficacy [15]. This highlights the need for new scaffolds, preferably derived from natural products, to address current therapeutic gaps [16].

Despite significant global progress in vaccination, complementary therapeutic approaches remain crucial for comprehensive COVID-19 management, particularly for unvaccinated individuals or those with weakened immunity [17]. Furthermore, the declining efficacy of currently approved antiviral agents against emerging variants [18] underscores the need to explore alternative antiviral scaffolds. Recent studies have identified several potent non-covalent Mpro inhibitors effective against Omicron and its subvariants [19–21], reinforcing the therapeutic relevance of targeting Mpro as a central viral enzyme.

Lippia javanica (Burm. f.), a medicinal herb native to Southeast Asia, has garnered interest due to its traditional use in treating respiratory ailments and its potential antiviral properties [22]. Known locally as "fever tea" or "koorsbossie," it was widely used during the pandemic, particularly in rural Zimbabwe [18]. Its infusion has been shown to suppress oxidative stress and allergic airway inflammation [23]. While limited data exist on its activity against SARS-CoV-2, related *Lippia* species have demonstrated in vitro antiviral effects against Zika, dengue, herpes simplex, and bovine viruses [24–26]. Recently, the potential of *Lippia alba* metabolites to be repurposed as anticoagulant therapeutics and inhibitors against the SARS-CoV-2 main protease (Mpro) was investigated in silico [27]. Generally, the *Lippia* genus is rich in essential oils, including myrcene, limonene, and carvacrol, as well as phenolics such as apigenin and verbascoside, all of which have demonstrated antiviral activity [28–30].

However, no study has directly evaluated *L. javanica*'s activity against SARS-CoV-2. To bridge this gap, we investigated 116 phytochemicals from *L. javanica* identified via LC-MS and previous literature [30] for their inhibitory potential against Omicron Mpro using in silico methods. We performed drug-likeness, toxicity, and bioactivity predictions, followed by molecular docking and dynamics simulations to evaluate binding interactions and stability. This work offers a novel perspective on the antiviral potential of *L. javanica*, particularly in targeting emerging SARS-CoV-2 variants. To our knowledge, this is the first study to explore *L. javanica* as a natural source of Mpro inhibitors against the Omicron variant, utilizing an integrated experimental and computational approach. In contrast to the previous study on *L. alba* [27] and other related studies [20, 21], the integration of LC-MS-based metabolomic profiling with comprehensive computational analysis ensures that experimentally detected L. javanica phytochemicals are evaluated, thereby enhancing the biological relevance and reliability of the predicted interactions. The workflow of this study is illustrated in (Supplementary Fig. 1).

2 Methodology

2.1 Preparation of *Lippia javanica* extract

Lippia javanica leaves were harvested in Westville, Durban, South Africa, and authenticated at the Department of Horticulture, Durban University of Technology, Durban, South Africa. Subsequently, the leaves were air-dried, pulverized using a blender, and

stored in airtight containers at 4 °C until further use. To extract the bioactive compounds, 10 g of the powdered leaves were suspended in distilled water (100 mL) and then boiled on a magnetic stirrer for 20 min. Afterward, the infusion was cooled to room temperature and filtered sequentially through Whatman No. 1 filter paper and a 0.20 µm syringe filter. The resulting filtrate was lyophilized and stored at -20 °C for future use.

2.2 liquid chromatography-mass spectrometry (LC-MS)

LC-MS analysis of the *L. javanica* aqueous extract was performed using a Waters Synapt G2 quadrupole time-of-flight high-definition mass spectrometer (Milford, MA, USA) linked to a Waters Acquity ultra-performance liquid chromatograph and Acquity photodiode array detector. Ionization was achieved using an electrospray source, with N2 serving as the desolvation gas. A Waters UPLC BEH C18 column was used for the separation, and the gradient followed, according to Kaigongi et al. (2020) [31], at a 0.4 mL min^{-1} flow rate. Compounds were relatively quantified against a calibration curve established using rutin as the standard. Peak alignments were then exported to MSFinder 3.5 for compound annotation, where the m/z ions (MS2 spectra) were aligned with those generated by in-silico fragmentation against the in-built database libraries [32].

2.3 ligand and protein preparation

Three-dimensional (3D) structures of 116 *L. javanica* metabolites and the reference drug nirmatrelvir (CID: 155903259) were retrieved from PubChem [33]. These ligands comprised 87 compounds identified via LC-MS (Sect. 2.2) and 29 additional compounds from a prior study [30], as listed in Supplementary Table S1. Three-dimensional (3D) structures were utilized over two-dimensional (2D) ones to accurately capture molecular geometry, spatial orientation, and interaction sites, which are essential for robust protein-ligand binding analyses [34]. The *L. javanica* phytochemicals were prepared using OpenBabel software [35]. The X-ray crystal structure of SARS-CoV-2 Omicron Main Protease (Mpro, PDB ID: 8HOZ) was obtained from the RCSB Protein Data Bank [36]. Protein structures were processed using UCSF Chimera, which involved removing water molecules, correcting non-standard residue names, and ensuring proper residue connectivity [37]. Although higher-resolution Omicron Mpro structures exist (e.g., 8HOM at 1.56 Å), 8HOZ (2.83 Å) was deliberately selected because it is the only available Omicron Mpro structure co-crystallized with nirmatrelvir, the reference standard inhibitor used in this study, as elucidated in Table 1. This allows for the direct overlay and comparison of binding modes between our phytochemicals and the clinically approved drug within the same protein conformation and crystal packing environment, thereby eliminating artifacts from ligand-induced conformational changes observed in apo or differently liganded structures. This approach is standard in benchmarking studies and has been employed in various investigations on Mpro inhibitors [19, 21].

2.4 Molecular docking

Molecular docking was performed using AutoDock Vina (version 1.1.2) integrated within PyRx (version 0.8) to screen 116 *L. javanica* phytochemicals against the catalytic site of SARS-CoV-2 Omicron Main Protease (Mpro, PDB: 8HOZ), with nirmatrelvir as the reference compound [38, 39]. The receptor grid box was set to 25.00 × 25.00 × 25.00 Å and centered at coordinates (-17.91, 14.78, -26.16) along the x, y, and z axes to

Table 1 Comparison of SARS-CoV-2 Omicron variant Mpro PDB structures used in recent studies

PDB ID	Resolution(Å)	Release Date	Mutation	Bound Ligand	Key Justification for Selection of 8HOZ
7TLL	1.63	2022-01-26	YES	None (apo)	High resolution but no co-crystallized inhibitor
8HOM	1.56	2023-12-13	YES	Ensitrelvir	Highest resolution but bound to ensitrelvir (not nirmatrelvir)
8RJZ	1.70	2024-05-29	NO	GUE-3801	Good resolution; ligand not clinically approved
8HOZ*	2.83	2023-03-01	YES	Nirmatrelvir	selected: the only Omicron Mpro structure co-crystallized with nirmatrelvir (Paxlovid), enabling direct, unbiased pose comparison despite lower resolution[19, 21].
8CYZ	1.90	2023-08-30	NO	Compound C4	Moderate resolution; non-clinical ligand

Table 2 Molecular Docking binding affinities (kcal/mol) of the top ten *Lippia Javanica* phytochemicals and nirmatrelvir against SARS-CoV-2 Omicron Mpro (PDB: 8HOZ)

Code	Ligand	Docking score 1	Docking Score 2	Docking score 3	Mean ± SD
LP53	Verbascoside	-8.4	-8.5	-8.6	-8.50 ± 0.08
LP54	Isoverbascoside	-9.2	-9.3	-9.4	-9.30 ± 0.08
LP58	Apigenin	-7.6	-7.5	-7.7	-7.60 ± 0.08
LP69	**Crassifolioside**	**-8.5**	**-8.5**	**-8.7**	**-8.57 ± 0.09**
LP70	Luteolin	-7.9	-7.8	-7.9	-7.87 ± 0.05
LP72	Chrysoeriol	-7.6	-7.7	-7.8	-7.70 ± 0.08
LP101	Secogalioside	-7.5	-7.5	-7.4	-7.47 ± 0.05
LP103	**6-DTCA**	-8.5	-8.6	-8.7	**-8.60 ± 0.08**
LP106	**4-OO**	-8.8	-8.7	-8.8	**-8.77 ± 0.05**
LP109	Monotropeine	-7.5	-7.7	-7.6	-7.60 ± 0.08
NIR	**Nirmatrelvir**	**-8.8**	**-8.5**	**-8.7**	**-8.67 ± 0.12**

*4-OO – 4-(1,3-Benzodioxol-5-ylmethylidene)-3-(3-nitrophenyl)-1,2-oxazol-5-one),

*6-DTCA – (6-(5,6-Dihydroxy-4-oxo-2-phenylchromen-7-yl)oxy-3,4,5-trihydroxyoxane-2-carboxylic acid)

*Values are mean ± SD from three independent docking runs using PyRx/AutoDock Vina (exhaustiveness = 8)

encompass the active site fully. Docking simulations were conducted with an exhaustiveness parameter of 8 and default ligand preparation settings. Gasteiger charges were assigned to all compounds, and non-polar hydrogen atoms were merged with their respective carbon atoms [40]. To ensure reproducibility and statistical robustness, the top 10 phytochemicals and nirmatrelvir were subjected to three fully independent docking runs with random seeding disabled between runs, generating statistically independent conformational sampling [39]. Binding affinities are reported as mean ± population standard deviation (SD) from these triplicate runs (n = 3). Raw PyRx output files and screenshots confirming independent runs are provided in Table 2. Predicted binding energies and protein-ligand interactions were visualized using BIOVIA Discovery Studio 2021 Client [41]. The highest-scoring phytochemicals were selected for subsequent physicochemical, toxicity, and molecular dynamics analyses, with full results presented in Supplementary Table S2.

2.5 Physicochemical properties, bioactivity, and toxicity prediction

The physicochemical properties of top-docked *Lippia javanica* ligands, including molecular weight, topological polar surface area (TPSA), hydrogen bond donors (HBD),

hydrogen bond acceptors (HBA), heavy atom count, partition coefficient (miLogP), and Lipinski's Rule of Five violations, were predicted alongside nirmatrelvir using SwissADME [42]. Additionally, the OSIRIS Property Explorer web tool (http://www.organic-chemistry.org/prog/peo/) was used to assess the potential toxicity risks, including mutagenicity, tumorigenicity, irritancy, and reproductive effects, of these compounds [43].

2.6 Molecular dynamics (MD) simulations

Molecular dynamics (MD) simulations were performed as described by Obakachi et al. [44], with slight modifications. All simulations were conducted using the GPU-accelerated version of the AMBER 18 package [39], which utilized the FF18SB variant of the AMBER force field to model protein parameters [45]. System setup was completed in the LEaP module, where hydrogen atoms and counterions (Na^+ and Cl^-) were added to neutralize the systems. Each complex was solvated in a rectangular TIP3P water box with a 10 Å buffer distance from any solute atom [46]. Energy minimization was conducted in two stages. First, 2,000 steps (1,000 steepest descent and 1,000 conjugate gradient) were applied under positional restraints of 500 kcal/mol on the solute. This was followed by an unrestrained minimization of 1,000 steps using the conjugate gradient method. The systems were then gradually heated from 0 to 300 K over 50 ps under the NVT ensemble, with 10 kcal/mol restraints on the solute and a Langevin collision frequency of 1.0 ps^{-1}. Subsequently, 500 ps of equilibration was performed under NPT conditions at 300 K and 1 bar, using the Berendsen barostat [47]. Production runs were carried out for 100 ns per complex. This duration was selected based on literature precedent to ensure sufficient sampling of conformational space and protein-ligand interaction stability [44, 48]. SHAKE constraints were applied to all bonds involving hydrogen atoms [44], with a 2 fs time step. The simulations employed SPFP precision under periodic boundary conditions. The pressure was maintained at 1 bar using the Berendsen barostat [47], with a pressure coupling constant of 2 ps. The Langevin thermostat was used to control the temperature at 300 K with a collision frequency of 1.0 ps^{-1} [49].

2.7 Post molecular dynamics analysis

The analyses of the Root Mean Square Deviation (RMSD), Radius of Gyration (RoG), Root Mean Square Fluctuation (RMSF), Solvent Accessible Surface Area (SASA), and hydrogen bond dynamics were carried out using the CPPTRAJ module of the AMBER 18 suite [50]. Visualization and raw data plotting were performed using Origin 6.0 software [51]. These structural and dynamic parameters were used to evaluate the stability, flexibility, and conformational behaviour of the protein-ligand complexes during the 100 ns simulation. To further quantify the binding strength of each complex, Molecular Mechanics/Generalized Born Surface Area (MM/GBSA) calculations were employed [52]. The binding free energies (ΔG_bind) were estimated from 10,000 snapshots extracted from the 100-ns MD trajectory, representing the last equilibrated portion of the simulation [53]. The energy contributions from the protein, ligand, and complex were decomposed into gas-phase interaction energies (electrostatic and van der Waals), solvation energies (polar and non-polar), and surface area energies. A per-residue energy decomposition (PRED) analysis was also performed to identify the key interacting

residues that contribute to the binding energy. The binding free energy (ΔG_bind) was computed using the standard MM/GBSA equation:

$$\Delta G_{bind} = G_{complex} - -G_{protein} - G_{inhibitor}$$

$$\Delta G_{bind} = E_{gas} + G_{sol} - TS$$

$$E_{gas} = E_{int} + E_{vdw} + E_{ele}$$

$$G_{sol} = G_{GB} + G_{SA}$$

$$G_{SA} = \gamma SASA$$

This method provides a balance between computational efficiency and accuracy, making it suitable for ranking binding affinities and elucidating interaction profiles of ligand candidates with the SARS-CoV-2 Omicron Mpro target.

3 Results and discussion

3.1 Bioactive components of *L . javanica*

The LC-MS analysis tentatively identified 87 secondary metabolites in the *L. javanica* aqueous extract (Supplementary file 1) with the Time-of-Flight Mass Spectrometer-Electrospray Ionization (TOF-MS-ESI) chromatogram of the analyte presented in Fig. 1. A broad classification of the detected compounds revealed their distribution across various categories, including terpenoids (17), phenolics (12), glycosides (11), amino acids and peptides (7), fatty acid derivatives (6), alkaloids (4), and others (30). The retention times of the identified compounds were recorded to be between 4.909 and 23.234 for uridine and citrusoside D, respectively (Supplementary file 1). Some of the major components in the extract include 7-Epi-12-hydroxyjasmonic acid glucoside (519.3 mg/L), allamandin (359.3 mg/L), cardiomanol (110.4 mg/L), gallocatechin (530.1 mg/L), monotropein (205.9 mg/L), tuberonic acid (478.5 mg/L), secologanic acid (126.1 mg/L), salicyclic acid glycoside (104.9 mg/L), secogaliosdie (433.5 mg/L), succinylglycerol (124.4 mg/L), tyrosine deriavative (238.2 mg/L), and verbascoside (238.2 mg/L). Several *L. javanica* compounds in this study aligned with the findings of previous studies [54–56]. For example, verbascoside, a highly bioactive glycoside, has been consistently identified as a major constituent of *L. javanica* leaf extracts [54, 55]. Interestingly, the antiviral properties of some of these detected compounds have been highlighted in various

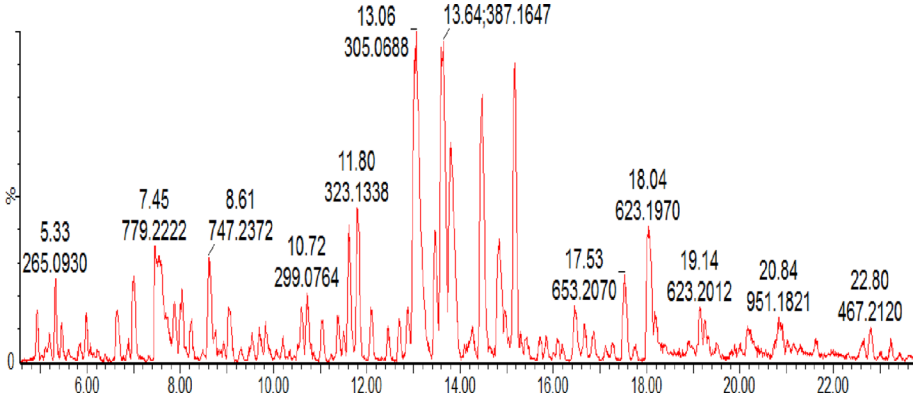

Fig. 1 Chromatogram of *Lippia javanica* aqueous extract

studies. To mention a few, verbascoside, isolated from *Lepechinia* species, demonstrated remarkable inhibitory activity against herpes simplex virus types 1 and 2 [52]. Apigenin has also been recently shown to ameliorate pseudo-SARS-CoV-2-induced inflammatory responses and pulmonary fibrosis [53], as well as inhibit SARS-CoV-2 in vitro [57]. Although local communities claim the plant has therapeutic effects against viral infections, there is currently no scientific data to substantiate these claims. However, other plants from the *Lippia* genus have been demonstrated to possess antiviral properties, such as *L. alba* [58] and *L. graveolens* [24].

3.2 Molecular docking analysis

The docking analysis evaluated the binding affinities of 116 Lippia javanica phytochemicals and the reference drug nirmatrelvir against the SARS-CoV-2 Omicron main protease (Mpro) (Supplementary Table S2), with binding scores ranging from – 3.4 kcal/mol (glycine) to -9.30 ± 0.08 kcal/mol. To ensure reproducibility and statistical robustness, the top 10 phytochemicals and nirmatrelvir were re-docked twice using PyRx (AutoDock Vina 1.2) with independent random seeding after initial virtual screening. Binding energies, expressed as the mean ± standard deviation (SD) from three independent runs, are summarized in Table 2. The table lists the top 10 ligands with their respective binding affinities, while their corresponding 2D chemical structures are illustrated in Fig. 2. Isoverbascoside emerged as the most potent inhibitor, exhibiting a significantly higher affinity (-9.30 ± 0.08 kcal/mol) than nirmatrelvir (-8.67 ± 0.12 kcal/mol; $\Delta = 0.63$ kcal/mol, $p = 0.003$, two-tailed t-test). Four additional compounds, 4-OO (-8.77 ± 0.05 kcal/mol), 6-DTCA (-8.60 ± 0.08 kcal/mol), crassifolioside (-8.57 ± 0.09 kcal/mol), and verbascoside (-8.50 ± 0.08 kcal/mol) also outperformed nirmatrelvir (all $p < 0.05$). The top-performing ligands belong to two major chemical classes: flavonoids (apigenin, chrysoeriol, luteolin, 6-DTCA) and phenylpropanoid glycosides (crassifolioside, isoverbascoside, secogalioside, verbascoside). Flavonoids have previously demonstrated antiviral activity against human coronaviruses and other pathogens in both in vitro and in vivo studies [59]. Notably, chrysoeriol suppresses SARS-CoV-2 entry by downregulating ACE2/TMPRSS2, NOX2, and MCP-1 [60]. Among the glycosides, verbascoside is well-documented for its potent inhibition of herpes simplex virus types 1 and 2 [61]. These

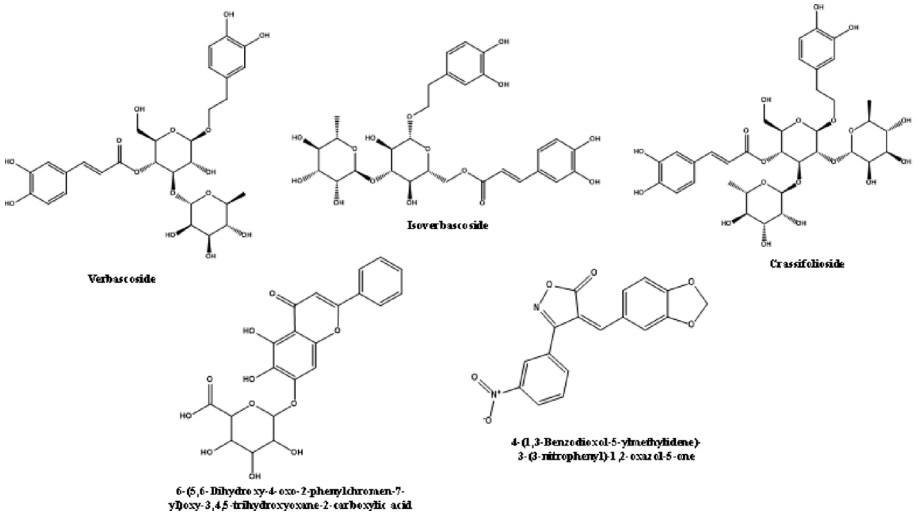

Fig. 2 Chemical structures of the 5-lead *Lippia javanica* ligands

results strongly support the superior binding potential of *L. javanica* phytochemicals, particularly isoverbascoside, as promising Mpro inhibitors compared to the clinically approved nirmatrelvir.

This study further elucidated the molecular interactions between the *L. javanica* phytochemicals and the amino acid residues within the binding site of the Mpro. Binding interactions, including the strong hydrogen bond (H-bond), alkyl, π-alkyl, π-π stacked, π-π T-shaped interactions, and Van der Waals (vdW) overlapping between the ligands and protein (Fig. 3). The molecular interaction plot between the *L. javanica* phytochemicals and Mpro showed that the phytochemicals compete favourably with nirmatrelvir, while most exhibited more interactions than the reference drug.

(Fig. 3). In this regard, crassifolioside, isoverbascoside, verbascoside, 6-DTCA, and 4-OO had 28, 27, 25, 20, and 17 interactions, respectively, compared to nirmatrelvir's 26. Furthermore, crassifolioside, verbascoside, and isoverbascoside exhibited higher numbers of hydrogen bonds (11, 10, and 9, respectively) than nirmatrelvir (6), thus suggesting enhanced binding stability with the Mpro. Alkyl and π-alkyl interactions, particularly in crassifolioside (4) and isoverbascoside (1 π-sigma), further reinforced hydrophobic contacts, contributing to their strong van der Waals energies. Additionally, π-π stacking interactions in isoverbascoside and 6-DTCA added to the stability of these complexes. These interactions likely contribute to the high binding free energies, highlighting the potential of these compounds as potent inhibitors of SARS-CoV-2 Mpro. Also, the varying nature and quantity of these interactions, particularly the increased number of hydrogen bonds and π-type contacts, suggest not only enhanced binding stability but also improved specificity and stronger inhibition potential. Hydrogen bonds help anchor the ligands within the binding pocket, while π-π stacking and hydrophobic interactions strengthen the non-covalent retention of the ligands. These features likely contribute to longer residence time and reduced off-target binding, supporting the promise of these phytochemicals as highly selective Mpro inhibitors.

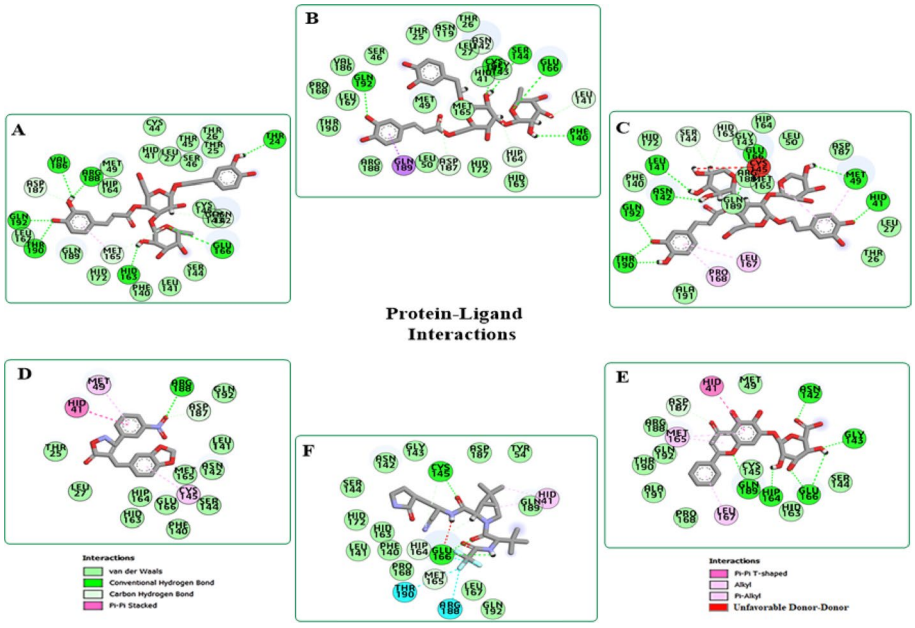

Fig. 3 Molecular interaction plots of SARS-CoV-2 Omicron Main Protease amino acid residues with **A** verbascoside, **B** isoverbascoside, **C** crassifolioside, **D** 6-DTCA, **E** 4-OO, **F** nirmatrelvir

3.3 Physicochemical properties, bioactivity, and toxicity prediction

The Lipinski Rule of Five (Ro5) evaluates drug-likeness based on molecular weight (≤ 500 g/mol), lipophilicity (LogP ≤ 5), the number of heavy atoms, hydrogen bond donors (HBD ≤ 5), and hydrogen bond acceptors (HBA ≤ 10) [62]. While nirmatrelvir adhered strictly to Ro5, it was observed that some of the *L. javanica* compounds exhibited some violations; in particular, verbascoside, isoverbascoside, and crassifolioside violated three out of the five rules as they exceeded the molecular weight limit, and possessed excessive HBAs and HBDs, which could hinder membrane permeability and oral bioavailability (Table 3). For example, verbascoside, with its molecular weight of 624.59 g/mol, which is due to its many sugar and aromatic moieties, exceeded the threshold of 500 g/mol, while its numerous hydroxyl groups, especially from its disaccharide, caffeic acid, and hydroxytyrosol moieties ensures that it violate the hydrogen bond donors > 5 and hydrogen bond acceptors > 10 rules. Similarly, crassifolioside, a phenylethanoid glycoside with a molecular weight of 742.68 g/mol, which is due to its glycosidic sugar and phenylethanoid core exceeded the threshold of 500 g/mol, in addition, these rich hydroxylated structural components are also responsible for its numerous hydroxyl groups, which also ensures that it violate the hydrogen bond donors > 5 and hydrogen bond acceptors > 10 rules. Some glycosidic compounds are known for their significant antiviral properties, despite violating the Ro5; a notable example is glycyrrhizin, which has been studied for its antiviral activity against viruses such as Hepatitis C, HIV, and SARS-CoV-2, despite violating three of the five rules [63].

However, the *L. javanica* compounds showed favourable lipophilicity with lower LogP values than nirmatrelvir, potentially improving water solubility and reducing nonspecific hydrophobic interactions. On the other hand, 4-OO was compliant with all of the 5's, while 6-DTCA violated only one of the rules. Despite the recorded violations, the compounds offer unique physicochemical profiles that may enhance their interaction with specific biological targets. Thus, *L. javanica* compounds, such as 6-DTCA, with fewer violations, could serve as starting points for lead optimization through strategies like prodrug development or alternative delivery systems, leveraging their potential benefits against the limitations posed by Ro5. Many natural products that violate Lipinski's rules have been known to elicit their therapeutic activities via non-oral routes or through metabolic transformation in the body. For instance, Bockus and McEwen [64] demonstrated that some natural cyclic peptides exhibit potent biological activities and can penetrate cells despite violating these rules. Generally, these compounds exhibit their bioactivity because they are typically hydrolyzed into their sugar and aglycone units

Table 3 Drug likeness scores of *Lippia Javanica* phytochemicals

Ligand	miLogP	TPSA	nHAtoms	HBA	HBD	Vol	M.wt	nviol
Verbascoside	-0.60	245.29	44	15	9	148.42	624.59	3
Isoverbascoside	-0.49	245.29	44	15	9	148.42	624.59	3
Crassifolioside	-2.17	304.21	52	19	11	170.03	742.68	3
6-DTCA	0.22	187.12	32	11	6	106.72	446.36	1
4-OO	2.28	102.94	25	7	0	91.70	338,0.27	0
Nirmatrelvir	1.89	131.40	35	8	3	499.53	499.53	0

** Lipophilicity (miLogP), polar surface area (TPSA), heavy atom count (nHAtoms), hydrogen bond acceptors (HBA), hydrogen bond donors (HBD), molecular volume (Vol), molecular weight (M.wt), and Lipinski's rule violations (nviol);

*4-OO – 4-(1,3-Benzodioxol-5-ylmethylidene)-3-(3-nitrophenyl)-1,2-oxazol-5-one),

*6-DTCA – (6-(5,6-Dihydroxy-4-oxo-2-phenylchromen-7-yl)oxy-3,4,5-trihydroxyoxane-2-carboxylic acid)

(active portions) in the body. Additionally, their administration via non-oral routes also circumvents the hurdle of oral absorption.

The toxicological profiles of *L. javanica* phytochemicals and the reference compound nirmatrelvir were assessed using the OSIRIS Property Explorer. This tool evaluates potential risks for mutagenicity, tumorigenicity, irritancy, and reproductive toxicity based on fragment-based rules derived from chemical substructures. While OSIRIS predictions are theoretical and not grounded in experimental datasets, the tool remains widely used for early-stage toxicity screening in drug discovery [65, 66]. The results, summarized in Table 4, indicate that several of the tested phytochemicals, including verbascoside, isoverbascoside, crassifolioside, and 6-DTCA, did not exhibit any toxicity risks in the evaluated parameters, suggesting favourable safety profiles. In contrast, the reference drug nirmatrelvir showed concerning toxicity alerts, particularly for tumorigenicity and irritancy, which may impact its long-term safety. One compound, 4-OO, flagged potential risks for mutagenicity and reproductive toxicity, indicating the need for further in-depth toxicological assessment.

3.4 Bioactivity prediction and quality assessment

To assess the bioactivity of selected ligands from *L. javanica*, the inhibitory constants (Ki) of the *L. javanica* compounds were computed using the standard equation $K_i = e^{-\Delta G/RT}$ where ΔG represents the binding energy obtained from molecular docking studies, R is the gas constant (1.987 × 10^-3 kcal/K-mol), and T is the absolute temperature (298.15 K) [67]. A low Ki value strongly indicates a compound's potential as a lead molecule [68]. Isoverbascoside was observed to possess the lowest Ki value, suggesting it has the highest potential as a lead inhibitor of Mpro (Table 5). Furthermore, the ligand efficiency (LE) computation showed that all ligands except 4-OO possessed values lower than the threshold value of 0.29 kcal/mol/HA. According to Schultes et al. [69], Lead-like molecules should ideally have LE values less than 0.29 kcal/mol/HA. However, it has been noted that LE is influenced by molecular size, which prompted the introduction of the ligand efficiency scale (LE scale), which is independent of ligand size [68]. A LE scale value below 0.4 indicates that a compound may exhibit potent inhibitory effects against an enzyme [69]. As shown in Table 4, all the lead ligands have LEscale values below 0.4, suggesting their potential effectiveness as inhibitors of catalytic function. The fit quality (FQ) is defined as the ligand efficiency (LE) ratio to the LE scale (LEscale), with values approaching 1 indicating stronger ligand-receptor interactions [70]. The calculation of the FQ for each lead compound revealed that both isoverbascoside and crassifolioside had FQ values of 1, while other compounds showed values close to 1 but required further

Table 4 OSIRIS toxicity risk assessment of *Lippia Javanica* phytochemicals

Ligand	Mutagenicity	Tumorigenicity	Irritability	*RE
Verbascoside	No	No	No	No
Isoverbascoside	No	No	No	No
Crassifolioside	No	No	No	No
6-DTCA	No	No	No	No
4-OO	Yes	No	No	Yes
Nirmatrelvir	No	Yes	Yes	No

*RE - Reproductive effects

*4-OO – 4-(1,3-Benzodioxol-5-ylmethylidene)-3-(3-nitrophenyl)-1,2-oxazol-5-one),

*6-DTCA – (6-(5,6-Dihydroxy-4-oxo-2-phenylchromen-7-yl)oxy-3,4,5-trihydroxyoxane-2-carboxylic acid)

Table 5 Bioactivity prediction of *Lippia Javanica* phytochemicals

Ligand	BE/DS	Ki	LE	LE_{SCALE}	FQ	LELP
Verbascoside	-8.4	0.69	0.19	0.21	0.90	-3.16
Isoverbascoside	-9.2	0.18	0.21	0.21	1.00	-2.33
Crassifolioside	-8.5	0.59	0.16	0.16	1.00	13.56
6-DTCA	-8.5	0.59	0.27	0.32	0.84	-0.82
4-OO	-8.8	0.70	0.35	0.39	0.89	-6.51
Nirmatrelvir	-8.8	0.70	0.25	0.40	0.63	-7.56

BE-Binding energy/ DS-Docking score; Ki-Predicted inhibition constant; LE-Ligand efficiency; LE_{SCALE} - Ligand efficiency scale; FQ - Fit quality; LELP ligand-efficiency-dependent lipophilicity

*4-OO – 4-(1,3-Benzodioxol-5-ylmethylidene)-3-(3-nitrophenyl)-1,2-oxazol-5-one), *6-DTCA – (6-(5,6-Dihydroxy-4-oxo-2-phenylchromen-7-yl)oxy-3,4,5-trihydroxyoxane-2

refinement. In contrast, the reference drug nirmatrelvir had an FQ value far less than 1 (Table 5). The strong FQ values for isoverbascoside and crassifolioside suggest they may exhibit optimal binding characteristics, warranting deeper exploration into their potential as effective therapeutic agents against the SARS-CoV-2 Omicron variant. Similarly, the lipophilic efficiency of ligand binding (LELP) values for the lead compounds provide insight into the balance between binding efficiency and lipophilicity. Among the ligands analysed, crassifolioside stands out with a remarkably high LELP value of 13.56, indicating a strong balance between its binding efficiency and lipophilicity, making it a promising candidate for further investigation. In contrast, nirmatrelvir and 4-OO exhibit significantly negative LELP values of -7.56 and – 6.51, respectively, reflecting less favourable profiles regarding binding efficiency relative to their lipophilic characteristics. Additionally, isoverbascoside, verbascoside, and 6-DTCA display negative LELP values of -2.33, -3.16, and – 0.82, respectively. These values suggest that while these compounds may have good binding efficiency, they require optimization to enhance their lipophilicity for improved therapeutic potential.

3.5 Molecular dynamics (MD) simulation of SARS-CoV-2 Omicron Mpro protein-ligand complexes

MD simulation is considered a critical approach in elucidating the dynamic behaviour as well as the stability of ligands during their interaction with protein targets [71, 72]. Thus, the all-atom MD simulations carried out in this study show the conformational sampling of the unbound SARS-CoV-2 Omicron Mpro (apoprotein) and complexes formed with the best-performing ligands as observed in the Root Mean Square Deviation (RMSD), Root Mean Square Fluctuation (RMSF), Radius of Gyration (RoG), Solvent Accessible Surface Area (SASA), and Hydrogen bonding plots (Fig. 4) and Table 6 showing their averages of these parameters. Furthermore, the binding energies of SARS-CoV-2 Mpro-ligand interactions, as well as the various components of these energies, provided insight into the different protein-ligand interactions observed in this study (Table 7).

3.5.1 Dynamic stability and flexibility of SARS-CoV-2 Omicron Mpro

The RMSD analysis, which assesses the overall structural stability of protein-ligand complexes, revealed that all systems remained stable throughout the simulation, with average deviations of less than 3.5 Å. The apo-Mpro exhibited a baseline RMSD of 1.55 Å, while nirmatrelvir and isoverbascoside complexes showed slightly higher values of 2.04 Å and 2.34 Å, respectively, indicating stable binding with moderate structural fluctuation (Fig. 4A). Additionally, crassifolioside induced the lowest deviation among the ligands (1.63

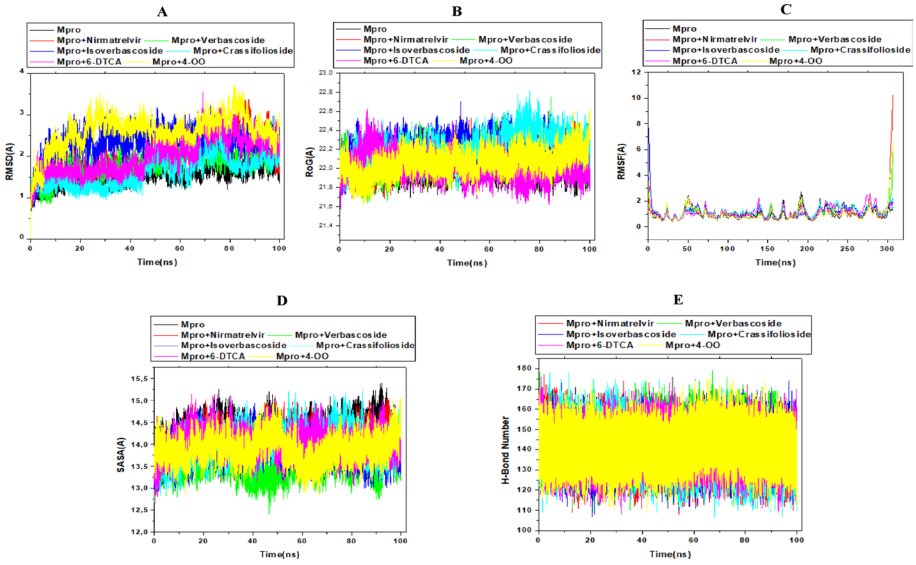

Fig. 4 Comparative **A** RMSD, **B** RoG, **C** RMSF, **D** SASA, and **E** H-Bond Number profile plots of C-α atoms of SARS-CoV-2 Omicron Main Protease (Mpro) with nirmatrelvir, verbascoside, isoverbascoside, crassifolioside, 6-DTCA, and 4-OO ligands

Table 6 Average values of parameters used to interpret structural stability for SARS-CoV-2 Omicron Mpro

Complex	RMSD (Å)	RoG (Å)	RMSF (Å)	SASA(Å)	H-Bond Number
Mpro	1.55 ± 0.23	22.02 ± 0.09	0.94 ± 0.44	14.21 ± 0.29	-
Mpro + Nirmatrelvir	2.04 ± 0.45	22.11 ± 0.11	1.07 ± 0.51	14.08 ± 0.26	140.70 ± 8.02
Mpro + Verbascoside	1.82 ± 0.33	22.12 ± 0.12	1.18 ± 0.59	13.62 ± 0.27	142.93 ± 8.03
Mpro + Isoverbascoside	2.34 ± 0.33	22.21 ± 0.12	1.12 ± 0.43	13.91 ± 0.26	141.55 ± 7.55
Mpro + Crassifolioside	1.63 ± 0.37	22.22 ± 0.15	1.19 ± 0.43	14:03 ± 0.29	140.61 ± 8.34
Mpro + 6-DTCA	2.01 ± 0.43	22.02 ± 0.12	1.14 ± 044	14.04 ± 0.27	141.50 ± 7.73
Mpro + 4-OO	2.59 ± 0.40	22.07 ± 0.12	1.00 ± 0.64	13.90 ± 0.28	142.03 ± 7.73

Table 7 Thermodynamic binding free energy profiles for the Mpro-ligand complexes

Complex	Nirmatrelvir	Verbascoside	Isoverbascoside	Crassifolioside	6-DTCA	4-OO
Binding energy (kcal/mol)						
ΔE_{vdW}	-52.65 ± 4.05	-68.79 ± 4.14	-68.73 ± 5.90	-68.49 ± 5.62	-45.51 ± 5.49	-41.52 ± 2.79
ΔE_{elec}	-11.05 ± 5.28	-21.95 ± 8.48	-51.41 ± 20.38	-31.42 ± 11.80	25.35 ± 12.87	-18.26 ± 4.58
ΔG_{gas}	-63.70 ± 6.87	-90.74 ± 9.44	-120.13 ± 22.07	-99.92 ± 11.24	-20.16 ± 15.70	-59.78 ± 5.29
ΔG_{solv}	29.02 ± 4.88	44.20 ± 6.30	61.97 ± 13.41	51.80 ± 7.22	-10.98 ± 12.33	26.49 ± 3.50
ΔG_{bind}	-34.68 ± 3.71	-46.54 ± 4.91	-58.16 ± 9.65	-48.12 ± 5.79	-31.14 ± 5.58	-33.29 ± 2.85

Å), suggesting a structural behaviour closely aligned with the unbound protein. The RoG analysis, on the other hand, which reflects protein compactness [73], showed minimal variation across all systems, with values ranging from 22.02 Å (apo and 6-DTCA) to 22.22 Å (crassifolioside), indicating that ligand binding did not significantly alter the structural compactness of Mpro (Fig. 4B). These consistent RoG values suggest that both the reference and plant-derived compounds preserved the overall structural stability of the protein. RMSF profiles indicated localized flexibility, with values ranging from 1.00 Å (4-OO) to 1.19 Å (crassifolioside). Isoverbascoside showed moderate residue fluctuation (1.14 Å), comparable to nirmatrelvir (1.07 Å), suggesting preserved residue stability across key regions (Fig. 4C). SASA values supported this trend. The apo-protein

recorded 14.21 Å², while isoverbascoside (13.67 Å²) and other lead compounds exhibited slightly reduced solvent exposure, reflecting enhanced binding compactness and structural integrity (Fig. 4D; Table 6). Hydrogen bonding analysis showed strong and consistent interactions across all complexes. Isoverbascoside formed 142.39 hydrogen bonds, nearly matching verbascoside (142.93) and exceeding the reference compound nirmatrelvir (140.70), indicating robust and stable protein-ligand binding (Fig. 4E). Collectively, these metrics confirm that isoverbascoside maintains protein structural stability and forms strong binding interactions, reinforcing its potential as a promising SARS-CoV-2 Mpro inhibitor.

3.5.2 Evaluation of the binding energies of SARS-CoV-2 Omicron main protease-ligand interactions

The binding energy analysis of SARS-CoV-2 Omicron Mpro with the *L. javanica* compounds (verbascoside, isoverbascoside, crassifolioside, 6-DTCA, and 4-OO) revealed the competitive binding potential of the plant-derived ligands with respect to the reference drug, nirmatrelvir (Table 7). Isoverbascoside exhibited the strongest binding free energy (-58.16 kcal/mol), significantly surpassing nirmatrelvir (-34.68 kcal/mol). Similarly, verbascoside (-46.54 kcal/mol) and crassifolioside (-48.12 kcal/mol) also demonstrated superior binding energies compared to the reference drug, highlighting the potential of the *L. javanica* compounds as Mpro inhibitors. The thermodynamic profiles suggest that the enhanced stability of the plant compounds is primarily driven by strong van der Waals (vdW) interactions, with isoverbascoside possessing the highest vdW contribution (-68.73 kcal/mol). Additionally, isoverbascoside displayed enhanced electrostatic interactions (-51.41 kcal/mol), further contributing to its strong binding affinity. Comparatively, the electrostatic interactions for nirmatrelvir were weaker (-11.05 kcal/mol). The gas-phase free energy (ΔGgas) calculations corroborated these findings, with isoverbascoside demonstrating the most stable gas-phase binding energy (-120.13 kcal/mol), followed by crassifolioside (-99.92 kcal/mol) and verbascoside (-90.74 kcal/mol) in comparison to nirmatrelvir (-63.70 kcal/mol). Despite partially offsetting these favourable interactions, solvation energy (ΔGsolv) was highest for isoverbascoside (61.97 kcal/mol), reflecting its stability in the solvent environment, while nirmatrelvir displayed a lower solvation energy (29.02 kcal/mol), indicating reduced compensation for its gas-phase binding. These findings position isoverbascoside, crassifolioside, and verbascoside as the most promising *L. javanica* compounds against the SARS-CoV-2 Mpro protein, offering the potential for further therapeutic development.

To further compare the key parameters in this study, Table 8 summarizes the comparative performance of the top three L. javanica phytochemicals versus nirmatrelvir. Isoverbascoside exhibited the strongest binding (-58.16 ± 9.65 kcal/mol), surpassing nirmatrelvir by 23.48 kcal/mol ($p < 0.001$), corresponding to a predicted Ki of 0.18 nM, approximately 400-fold tighter binding. Crassifolioside and verbascoside also

Table 8 Comparison of key parameters for the top three phytochemicals vs. Nirmatrelvir

Compound	ΔGbind ± SD (kcal/mol)	Predicted Ki (nM)	Avg RMSD (Å)	H-bond Count
Isoverbascoside	-58.16 ± 9.65	0.18	2.34	24
Crassifolioside	-48.12 ± 5.79	0.59	1.63	30
Verbascoside	-46.54 ± 4.91	0.69	1.82	24
Nirmatrelvir	-34.68 ± 3.71	0.70	2.07	11

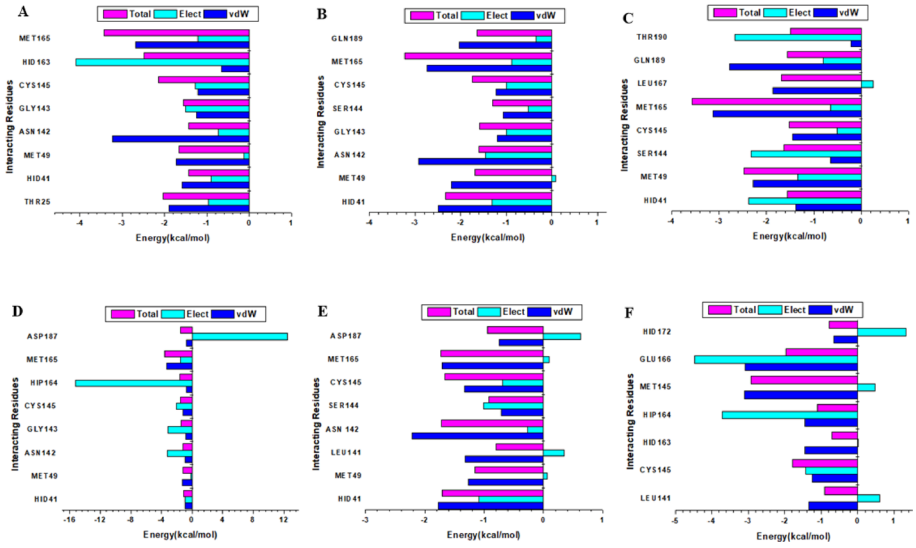

Fig. 5 Per-residue decomposition energy plot of SARS-CoV-2 Omicron Mpro in complex with the ligands: **A** verbascoside, **B** isoverbascoside, **C** crassifolioside, **D** 6 DTCA, **E** 4-OO, and **F** nirmatrelvir

outperformed nirmatrelvir by 13.44 and 11.86 kcal/mol, respectively. All three phytochemicals formed ≥ 24 stable hydrogen bonds (occupancy ≥ 70%), more than double that of nirmatrelvir (11), contributing to enhanced anchoring within the Mpro catalytic pocket.

3.5.3 Per-residue decomposition energy (PERD) analysis of SARS-CoV-2 Omicron Mpro and mechanistic insight

Per-residue energy decomposition via the MM/GBSA method reveals the individual amino-acid contributions to the total binding free energy and clarifies the molecular mechanism underlying Mpro inhibition. Figure 5 displays the top contributing residues for each complex as bar charts averaged across the 100 ns trajectories [51, 74]. Per-residue energy decomposition, as shown in Fig. 5, revealed that His41, Cys145, Met165, and Glu166 were the most influential residues contributing to ligand stabilization within the active site (Fig. 5). These residues define the catalytic core and substrate-binding architecture of Mpro, explaining their critical energetic roles. His41 and Cys145 constitute the catalytic dyad responsible for nucleophilic attack during peptide bond hydrolysis. The strong negative vdW and electrostatic contributions observed for these residues, particularly for isoverbascoside and verbascoside (-1.6 to -2.3 kcal·mol^{-1}), suggest that the ligands form tight, non-covalent contacts that could impede dyad polarization and block substrate access, thereby inhibiting catalysis. Glu166, which stabilizes substrate recognition at the S1 subsite, exhibited notable electrostatic interactions with all lead compounds, consistent with the formation of persistent hydrogen bonds that help lock the enzyme in an inactive conformation. Similarly, Met165, which forms the hydrophobic wall of the S2 pocket, showed dominant van der Waals (vdW) contributions (≈ -3.0 kcal·mol^{-1}) across the leads, reflecting close shape complementarity and enhanced hydrophobic packing. Stronger van der Waals (vdW) interactions denote an optimal steric fit and greater dispersion stabilization, which collectively improve binding affinity and inhibitory potential. By simultaneously anchoring to Glu166 and the catalytic dyad while maximizing van der Waals (vdW) contacts with Met165, the Lippia javanica

phytochemicals achieve both structural complementarity and catalytic interference. This combination likely underpins their lower predicted Ki and more favourable ΔG_bind relative to nirmatrelvir, signifying potent inhibition driven by synergistic hydrophobic and electrostatic stabilization within the catalytic pocket. These findings align with recent Omicron-specific docking studies [75, 76].

4 Conclusion

The COVID-19 pandemic highlighted the urgent need for innovative therapeutics to combat highly transmissible and immune-evasive SARS-CoV-2 variants, particularly the Omicron variant. This study is the first to investigate the inhibitory potential of Lippia javanica phytochemicals against the SARS-CoV-2 Omicron main protease (Mpro), a critical enzyme in viral replication. Among the screened compounds, isoverbascoside exhibited the most favourable binding free energy (-58.16 ± 9.65 kcal/mol), outperforming the reference inhibitor nirmatrelvir (-34.68 ± 3.71 kcal/mol). Verbascoside and crassifolioside also showed strong binding profiles. Molecular dynamics simulations confirmed the stability of these ligand-Mpro complexes, with consistent root mean square deviation (RMSD), root mean square fluctuation (RMSF), and radius of gyration (RoG) values indicating minimal structural perturbation. Toxicological assessments predicted low risks of mutagenicity and reproductive toxicity for the key phytochemicals, further supporting their therapeutic viability. Overall, these findings highlight L. javanica phytochemicals, particularly isoverbascoside, as promising leads for the development of novel small-molecule antivirals against Omicron and other emerging SARS-CoV-2 variants. Nonetheless, experimental validation through in vitro and in vivo studies is essential to confirm these computational insights and substantiate the traditional medicinal uses of L. javanica.

Supplementary Information

The online version contains supplementary material available at https://doi.org/10.1007/s44371-025-00430-6.

Supplementary Material 1

Acknowledgements

The authors thank the Department of Chemical Sciences, Faculty of Science, University of Johannesburg, South Africa, and the Centre for High-Performance Computing, CHPC South Africa, for providing all the necessary facilities and resources.

Statement on studies involving plants

The study adhered to WHO guidelines for good agricultural and collection practices (GACP) for medicinal plants. The collection of *Lippia javanica* leaves was conducted in full compliance with the National Environmental Management: Biodiversity Act of South Africa, and permission for collection was obtained from the Ezemvelo KZN Wildlife, South Africa. The *L. javanica* leaves used in this study were collected from Westville North, near Pinetown, KwaZulu-Natal, and authenticated by Mr. Thagan Anumanthoo, Senior Horticulturist at the Department of Horticulture, Durban University of Technology, Durban, South Africa. A voucher specimen of the plant material was assigned deposition number (F.O. Shode/15), preserved, and deposited at The Bews Herbarium, University of KwaZulu-Natal, Pietermaritzburg, South Africa.

Author contributions

Vincent Obakachi: Investigation, Formal analysis, Writing - original draft; Ayodeji Amobonye: Investigation, Formal analysis, Writing - original draft; Santhosh Pillai: Writing - review & editing; Krishna Govender: Writing - review & editing; Penny Govender: Writing - review & editing; Francis O. Shode: Conceptualization, Formal analysis, Conceptualization, Funding acquisition. All authors read and approved the final manuscript. The first two authors contributed equally to this work.

Funding

This research received no specific grant from funding agencies in the public, commercial, or not-for-profit sectors.

Data availability

All data generated or analysed during this study are included in this published article and its supplementary information files.

Declarations

Ethics approval and consent to participate
Not applicable.

Competing interests
The authors declare no competing interests.

Received: 5 July 2025 / Accepted: 14 December 2025
Published online: 24 December 2025

References

1. Garriga C, Valero-Gaspar T, Rodriguez-Blazquez C, Diaz A, Bezzegh P, Daňková Š, Unim B, Palmieri L, Thiβen M, Pentz R. Identification of methodological issues regarding direct impact indicators of COVID-19: a rapid scoping review on morbidity, severity and mortality. Eur J Public Health. 2024;34:i3–10. https://doi.org/10.1093/eurpub/ckae072. (Supplement_1).
2. Worldometer, COVID–19 Coronavirus Pandemic., Available from: https://www.worldometers.info/coronavirus/ (2004). https://doi.org/
3. Maurice RL. Post-COVID-19: time to change our way of life for a better future. Epidemiologia. 2024;5(2):211–20. https://doi.org/10.3390/epidemiologia5020015.
4. McKay T, Robinson RS, Musungu S, Padi-Adjirackor NA, Angotti N. The missing millions: Uncovering the burden of Covid-19 cases and deaths in the African Region, Popul. Dev Rev. 2024;50(1):7–58. https://doi.org/10.1111/padr.12608.
5. IDRIS IA. Emergence and spread of JN. 1 COVID-19 variant. Bull Natl Res Centre. 2024;48:27.
6. Chung Y-S, Lam C-Y, Tan P-H, Tsang H-F, Wong S-CC. Comprehensive review of COVID-19: epidemiology, pathogenesis, advancement in diagnostic and detection techniques, and post-pandemic treatment strategies. Int J Mol Sci. 2024;25(15):8155. https://doi.org/10.3390/ijms25158155.
7. André S, Bruyneel A-V, Chirumberro A, Roman A, Claus M, Alard S, De Vos N, Bruyneel M. Health-related quality of life improves in parallel with FEV1 and 6-minute walking distance test at between 3 and 12 months in critical COVID-19 survivors. Am J Med Open. 2023;10:100055. https://doi.org/10.1016/j.ajmo.2023.100055.
8. Parums DV. A rapid global increase in COVID-19 is due to the emergence of the EG. 5 (Eris) subvariant of Omicron SARS-CoV-2. Med Sci Monitor: Int Med J Experimental Clin Res. 2023;29:e942244–1. https://doi.org/10.12659/MSM.942244.
9. Sarkar A, Omar S, Alshareef A, Fanous K, Sarker S, Alroobi H, Zamir F, Yousef M, Zakaria D. The relative prevalence of the Omicron variant within SARS-CoV-2 infected cohorts in different countries: a systematic review. Hum Vaccines Immunotherapeutics. 2023;19(1):2212568. https://doi.org/10.1080/21645515.2023.2212568.
10. Reuschl A-K, Thorne LG, Whelan MV, Ragazzini R, Furnon W, Cowton VM, De Lorenzo G, Mesner D, Turner JL, Dowgier G. Evolution of enhanced innate immune suppression by SARS-CoV-2 Omicron subvariants. Nat Microbiol. 2024;9(2):451–63. https://doi.org/10.1038/s41564-023-01588-4.
11. Ao D, He X, Liu J, Xu L. Strategies for the development and approval of COVID-19 vaccines and therapeutics in the post-pandemic period. Signal Transduct Target Ther. 2023;8(1):466. https://doi.org/10.1038/s41392-023-01724-w.
12. Andrews HS, Herman JD, Gandhi RT. Treatments for COVID-19, annu. Rev Med. 2024;75(1):145–57. https://doi.org/10.1146/annurev-med-052422-020316.
13. Abe K, Kabe Y, Uchiyama S, Iwasaki YW, Ishizu H, Uwamino Y, Takenouchi T, Uno S, Ishii M, Maruno T. Pro108Ser mutation of SARS-CoV-2 3CLpro reduces the enzyme activity and ameliorates the clinical severity of COVID-19. Sci Rep. 2022;12(1):1299. https://doi.org/10.1038/s41598-022-05424-3.
14. Zagórska A, Czopek A, Fryc M, Jończyk J. Inhibitors of SARS-CoV-2 main protease (Mpro) as anti-coronavirus agents. Biomolecules. 2024;14(7):797. https://doi.org/10.3390/biom14070797.
15. Pagliano P, Spera A, Sellitto C, Scarpati G, Folliero V, Piazza O, Franci G, Conti V, Ascione T. Preclinical discovery and development of nirmatrelvir/ritonavir combinational therapy for the treatment of covid-19 and the lessons learned from SARS-cov-2 variants. Expert Opin Drug Discov. 2023;18(12):1301–11. https://doi.org/10.1080/17460441.2023.2248879.
16. Fischer C, Feys JR. SARS-CoV-2 Mpro inhibitors: achieved diversity, developing resistance and future strategies. Future Pharmacol. 2023;3(1):80–107. https://doi.org/10.3390/futurepharmacol3010006.
17. Lin J-G, Huang G-J, Su Y-C. Efficacy analysis and research progress of complementary and alternative medicines in the adjuvant treatment of COVID-19. J Biomed Sci. 2023;30(1):30. https://doi.org/10.1186/s12929-023-00923-5.
18. Vukovikj M, Melidou A, Nannapaneni P, Normark T, Kraus A, Broberg EK. Impact of SARS-CoV-2 variant mutations on susceptibility to monoclonal antibodies and antiviral drugs: a non-systematic review, April 2022 to October 2024. Eurosurveillance. 2025;30(10):2400252. https://doi.org/10.2807/1560-7917.ES.2025.30.10.2400252.
19. Zhou Y, Gammeltoft KA, Tjørnelund-Sjursen HD, Ryberg LA, Offersgaard A, Czarnota A, Duan Z, Pham LV, Fahnøe U, Peters GH. SARS-CoV-2 Mpro inhibitor ensitrelvir: asymmetrical cross-resistance with nirmatrelvir and emerging resistance hotspots. Emerg Microbes Infections. 2025;14(1):2552716. https://doi.org/10.1080/22221751.2025.2552716.
20. Ahmad F, Basharat Z, Janjua A, Najmi MH, Almajhdi FN, Hussain T, Ozsahin DU, Waheed Y. An exploratory binding study of molnupiravir efficacy against emerging Omicron SARS-CoV-2 variants. Sci Rep. 2025;15(1):36549. https://doi.org/10.1038/s41598-025-19353-4.
21. Okabe A, Carney DW, Tawada M, Akther T, Aida J, Takagi T, Dougan DR, Leffler AE, Bell JA, Frye L. Discovery of highly potent noncovalent inhibitors of SARS-CoV-2 main protease through Computer-Aided drug design. J Med Chem. 2025. https://doi.org/10.1021/acs.jmedchem.5c01199.
22. Mood K, Jogam P, Sirikonda A, Shekhawat MS, Rohela GK, Manokari M, Allini VR. Micropropagation, morpho-anatomical characterization, and genetic stability studies in lippia Javanica (Burm. f.) spreng: a multipurpose medicinal plant. Plant Cell Tissue Organ Cult (PCTOC). 2022;150(2):427–37. https://doi.org/10.1007/s11240-022-02294-5.
23. Mfengu MO, Shauli M, Engwa GA, Musarurwa HT, Sewani-Rusike CR. Lippia Javanica (Zumbani) herbal tea infusion attenuates allergic airway inflammation via Inhibition of Th2 cell activation and suppression of oxidative stress. BMC Complement Med Ther. 2021;21:1–14. https://doi.org/10.1186/s12906-021-03361-8.

24. Pilau MR, Alves SH, Weiblen R, Arenhart S, Cueto AP, Lovato LT. Antiviral activity of the lippia graveolens (Mexican oregano) essential oil and its main compound carvacrol against human and animal viruses. Braz J Microbiol. 2011;42:1616–24. https://doi.org/10.1590/S1517-83822011000400049.
25. Ocazionez RE, Meneses R, Torres FÁ, Stashenko E. Virucidal activity of Colombian lippia essential oils on dengue virus replication in vitro. Mem Inst Oswaldo Cruz. 2010;105:304–9. https://doi.org/10.1590/S0074-02762010000300010.
26. da Silva Sobrinho AR, Ramos LFS, Maciel YL, Maurício HdA, Cartaxo RdO, Ferreira SJ. Sette-de-Souza, orofacial features in children with microcephaly associated with Zika virus: A scoping review. Oral Dis. 2022;28(4):1022–8. https://doi.org/10.1111/odi.13804.
27. Yamari I, Abchir O, Siddique F, Zaki H, Errougui A, Talbi M, Bouachrine M, ElKouali Mh, Chtita S. The anticoagulant potential of lippia Alba extract in inhibiting SARS-CoV-2 mpro: density functional calculation, molecular Docking analysis, and molecular dynamics simulations. Sci Afr. 2024;23:e01986. https://doi.org/10.1016/j.sciaf.2023.e01986.
28. Pascual M, Slowing K, Carretero E, Mata DS, Villar A. Lippia: traditional uses, chemistry and pharmacology: a review. J Ethnopharmacol. 2001;76(3):201–14. https://doi.org/10.1016/S0378-8741(01)00234-3.
29. Shode F, Amobonye A, Olaseni J, Sabiu S, Govender K. Phytochemistry and Pharmacology potential of lippia javanica: a bibliometric and systematic review. Advancements Life Sci. 2025;12(1):23–34.
30. Maroyi A. Lippia Javanica (Burm. F.) Spreng.: traditional and commercial uses and phytochemical and Pharmacological significance in the African and Indian Subcontinent. Evidence-Based Complement Altern Med. 2017;2017(1):6746071. https://doi.org/10.1155/2017/6746071.
31. Kaigongi MM, Lukhoba CW, Ochieng ' PJ, Taylor M, Yenesew A, Makunga NP. LC-MS-Based metabolomics for the chemosystematics of Kenyan Dodonaea viscosa Jacq (sapindaceae) populations. Molecules. 2020;25(18):4130. https://doi.org/10.3390/molecules25184130.
32. Maluleke E, Jolly NP, Patterton HG, Setati ME. Antifungal activity of non-conventional yeasts against botrytis cinerea and non-Botrytis grape bunch rot fungi. Front Microbiol. 2022;13:986229. https://doi.org/10.3389/fmicb.2022.986229.
33. Kim S, Chen J, Cheng T, Gindulyte A, He J, He S, Li Q, Shoemaker BA, Thiessen PA, Yu B. PubChem 2023 update. Nucleic Acids Res. 2023;51(D1):D1373–80. https://doi.org/10.1093/nar/gkac956.
34. Goodsell DS, Zardecki C, Di Costanzo L, Duarte JM, Hudson BP, Persikova I, Segura J, Shao C, Voigt M, Westbrook JD. Protein Sci. 2020;29(1):52–65. https://doi.org/10.1002/pro.3730. RCSB Protein Data Bank: Enabling biomedical research and drug discovery.
35. O'Boyle NM, Banck M, James CA, Morley C, Vandermeersch T, Hutchison GR. Open babel: an open chemical toolbox. J Cheminform. 2011;3:1–14. https://doi.org/10.1186/1758-2946-3-33.
36. Burley SK, Bhikadiya C, Bi C, Bittrich S, Chao H, Chen L, Craig PA, Crichlow GV, Dalenberg K, Duarte JM, RCSB Protein Data Bank (RCSB. org): delivery of experimentally-determined PDB structures alongside one million computed structure models of proteins from artificial intelligence/machine learning. Nucleic Acids Res. 2023;51(D1):D488–508. https://doi.org/10.1093/nar/gkac1077.
37. Pettersen EF, Goddard TD, Huang CC, Couch GS, Greenblatt DM, Meng EC, Ferrin TE. UCSF Chimera—a visualization system for exploratory research and analysis. J Comput Chem. 2004;25(13):1605–12. https://doi.org/10.1002/jcc.20084.
38. Trott O, Olson AJ. AutoDock vina: improving the speed and accuracy of Docking with a new scoring function, efficient optimization, and multithreading. J Comput Chem. 2010;31(2):455–61. https://doi.org/10.1002/jcc.21334.
39. Dallakyan S, Olson AJ. Small-molecule library screening by Docking with pyrx. Chemical biology: methods and protocols. Springer; 2014. pp. 243–50.
40. Huey R, Morris GM, Forli S. Using AutoDock 4 and Vina with autodocktools: A tutorial. California, USA: Scripps Research Institute; 2011.
41. Nyijime TA, Shallangwa GA, Uzairu A, Umar AB, Ibrahim MT, Udofia IA, Obakachi VA, Govender KK. Computational design and evaluation of Hydrantoin derivatives as potential anti-tubercular agents: insight from ADMET, molecular docking, DFT, and molecular dynamic simulations. Lett Drug Des Discovery. 2025;100155. https://doi.org/10.1016/j.lddd.2025.100155.
42. Daina A, Michielin O, Zoete V. SwissADME: a free web tool to evaluate pharmacokinetics, drug-likeness and medicinal chemistry friendliness of small molecules. Sci Rep. 2017;7(1):42717. https://doi.org/10.1038/srep42717.
43. Sander T, Freyss J, von Korff M, Reich JR, Rufener C. OSIRIS, an entirely in-house developed drug discovery informatics system. J Chem Inf Model. 2009;49(2):232–46. https://doi.org/10.1021/ci800305f.
44. Obakachi VA, Kehinde I, Kushwaha ND, Akinpelu OI, Kushwaha B, Merugu SR, Kayamba F, Kumalo HM, Karpoormath R. Structural based investigation of novel pyrazole-thiazole hybrids as dual CDK-1 and CDK-2 inhibitors for cancer chemotherapy. Mol Simul. 2022;48(8):687–701. https://doi.org/10.1080/08927022.2022.2045016.
45. Nair PC, Miners JO. Molecular dynamics simulations: from structure function relationships to drug discovery. Silico Pharmacol. 2014;2:1–4. https://doi.org/10.1186/s40203-014-0004-8.
46. Jorgensen WL, Chandrasekhar J, Madura JD, Roger W, Impey, Klein ML. Comparison of simple potential functions for simulating liquid water. The Journal of chemical physics 79, no. 2 (1983): 926–935., J Chem Phys 79 (2) (1983) 926–935. https://doi.org/10.1063/1.445869
47. Basconi JE, Shirts MR. Effects of temperature control algorithms on transport properties and kinetics in molecular dynamics simulations. J Chem Theory Comput. 2013;9(7):2887–99. https://doi.org/10.1021/ct400109a.
48. MOHAMED RYOUSIF, ALMOGADDAM HM, ELAMIN MA, IBRAHIM KM, ALRADDADI SRMAINOUSAHBE, A. M., AWAD, E. A., ALZAIN AA. Computational screening campaign reveal natural candidates as potential ASK1 inhibitors: pharmacophore modeling, molecular docking, MMGBSA calculations, ADMET prediction, and molecular dynamics simulation studies. Sci Afr. 2025;28(e02634). https://doi.org/10.1016/j.sciaf.2025.e02634.
49. Loncharich BB, Pastor RJ. Langevin dynamics of peptides: The frictional dependence of isomerization rates of N-acetylalanyl-N'-methylamide. Biopolymers. 1992;32(5). https://doi.org/10.1002/bip.360320508. 523 – 35.
50. Case BK, Ben-Shalom DA, Brozell IY, Cerutti SR, Cheatham DS III et al. AMBER, University of California, San Francisco (2018).
51. Obakachi VA, Nchiozem-Ngnitedem V-A, Govender KK, Govender PP. In Silico exploration of natural Xanthone derivatives as potential inhibitors of severe acute respiratory syndrome coronavirus 2 (SARS-CoV-2) replication and cellular entry. J Comput -Aided Mol Des. 2025;39(1):7. https://doi.org/10.1007/s10822-025-00585-5.
52. Gapsys V, Michielssens S, Seeliger D, de Groot BL. Accurate and rigorous prediction of the changes in protein free energies in a large-scale mutation scan. Angew Chem Int Ed. 2016;55(26):7364–8. https://doi.org/10.1002/anie.201411811.

53. Shode FO, Uhomoibhi JO-o, Idowu KA, Sabiu S, Govender KK. Molecular dynamics study on selected bioactive phytochemicals as potential inhibitors of HIV-1 subtype C protease. Metabolites. 2022;12(11):1155. https://doi.org/10.3390/metabo12111155.
54. Madzimure J, Nyahangare ET, Hamudikuwanda H, Hove T, Stevenson PC, Belmain SR, Mvumi BM. Acaricidal efficacy against cattle ticks and acute oral toxicity of lippia Javanica (Burm F.) Spreng, trop. Anim Health Prod. 2011;43:481–9. https://doi.org/10.1007/s11250-010-9720-1.
55. Nina N, Burgos-Edwards A, Theoduloz C, Tripathy S, Matsabisa MG, Schmeda-Hirschmann G. Chemical Profiling, enzyme inhibitory activity and antioxidant capacity of South African herbal teas: buddleja saligna, lippia javanica, L. scaberrima and phyla dulcis. Antioxidants. 2024;13(10):1219. https://doi.org/10.3390/antiox13101219.
56. Suleman Z, Engwa GA, Shauli M, Musarurwa HT, Katuruza NA, Sewani-Rusike CR. Neuroprotective effects of lippia Javanica (Burm. F.) Spreng. Herbal tea infusion on Lead-induced oxidative brain damage in Wistar rats. BMC Complement Med Ther. 2022;22(1):4. https://doi.org/10.1186/s12906-021-03471-3.
57. Selim S, Albqmi M, Alanazi A, Alruwaili Y, Al-Sanea MM, Alnusaire TS, Almuhayawi MS, Al Jaouni SK, Hussein S, Warrad M. Antiviral activities of Olive oil apigenin and taxifolin against SARS-CoV-2 RNA-dependent RNA polymerase (RdRP): in silico, pharmacokinetic, ADMET, and in-vitro approaches. Cogent Food Agric. 2023;9(1):2236828. https://doi.org/10.1080/23311932.2023.2236828.
58. Sobrinho ACN, de Morais SM, Marinho MM, de Souza NV, Lima DM. Antiviral activity on the Zika virus and larvicidal activity on the Aedes spp. Of lippia Alba essential oil and β-caryophyllene. Ind Crops Prod. 2021;162:113281. https://doi.org/10.1016/j.indcrop.2021.113281.
59. Netshiluvhi TR. An exploratory review of commonly used plants in South Africa with promising Pharmacological effects on human coronaviruses and other viral infections. Nat Prod Commun. 2025;20(4):1934578X251313924. https://doi.org/10.1177/1934578X251313924.
60. Youn JY, Wang J, Li Q, Huang K, Cai H. Robust therapeutic effects on COVID-19 of novel small molecules: alleviation of SARS-CoV-2 S protein induction of ACE2/TMPRSS2, NOX2/ROS, and MCP-1. Front Cardiovasc Med. 2022;9:957340. https://doi.org/10.3389/fcvm.2022.957340.
61. Martins FO, Esteves PF, Mendes GS, Barbi NS, Menezes FS, Romanos MT. Verbascoside isolated from Lepechinia speciosa has inhibitory activity against HSV-1 and HSV-2 in vitro. Nat Prod Commun. 2009;4(12):1934578X0900401217. https://doi.org/10.1177/1934578X0900401217.
62. Kayamba F, Malimabe T, Ademola IK, Pooe OJ, Kushwaha ND, Mahlalela M, van Zyl RL, Gordon M, Mudau PT, Zininga T. Design and synthesis of quinoline-pyrimidine inspired hybrids as potential plasmodial inhibitors. Eur J Med Chem. 2021;217:113330. https://doi.org/10.1016/j.ejmech.2021.113330.
63. Sabiu S, Idowu K. An insight on the nature of biochemical interactions between glycyrrhizin, myricetin and CYP3A4 isoform. J Food Biochem. 2022;46(3):e13831. https://doi.org/10.1111/jfbc.13831.
64. Bockus AT, McEwen CM, Lokey RS. Form and function in Cyclic peptide natural products: a Pharmacokinetic perspective. Curr Top Med Chem. 2013;13(7):821–36. https://doi.org/10.2174/1568026611313070005.
65. Rushendran R, Singh A, Begum SRF, Chitra V, Ali N, Prajapati BG. Bioinformatics exploration of the therapeutic potential of Lotus seed compounds in multiple sclerosis: A network analysis of c-Jun pathway. Drug Dev Res. 2025;86(1):e70038. https://doi.org/10.1002/ddr.70038.
66. Amobonye A, Sabiu S, Olaleye MT, Pillai S. Computational investigation into parinari curatellifolia flavonoids as lead hepatoprotective therapeutics. J Appl Pharm Sci. 2024;14(11):167–77. https://doi.org/10.7324/JAPS.2024.188178.
67. Jedrzejas MJ, Singh S, Brouillette WJ, Air GM, Luo M. A strategy for theoretical binding constant, Ki, calculations for neuraminidase aromatic inhibitors designed on the basis of the active site structure of influenza virus neuraminidase. Proteins Struct Funct Bioinform. 1995;23(2):264–77. https://doi.org/10.1002/prot.340230215.
68. Reynolds CH, Reynolds RC. Group additivity in ligand binding affinity: an alternative approach to ligand efficiency. J Chem Inf Model. 2017;57(12):3086–93. https://doi.org/10.1021/acs.jcim.7b00381.
69. Schultes S, de Graaf C, Haaksma EE, de Esch IJ, Leurs R, Krämer O. Ligand efficiency as a guide in fragment hit selection and optimization. Drug Discovery Today: Technol. 2010;7(3):e157–62. https://doi.org/10.1016/j.ddtec.2010.11.003.
70. Adewumi AT, Oluyemi WM, Adekunle YA, Adewumi N, Alahmdi MI, Soliman ME, Abo-Dya NE. Propitious Indazole compounds as β-ketoacyl-ACP synthase inhibitors and mechanisms unfolded for TB cure: integrated rational design and MD simulations. ChemSelect. 2023;8(3):e202203877. https://doi.org/10.1002/slct.202203877.
71. Kushwaha B, Kushwaha ND, Priya M, Chandrasekaran B, Obakachi VA, Chauhan R, Kidwai S, Singh R, Ganai AM, Karpoormath R. Novel fluorophenyl tethered thiazole and chalcone analogues as potential anti-tubercular agents: design, synthesis, biological and in Silico evaluations. J Mol Struct. 2023;1276:134791. https://doi.org/10.1016/j.molstruc.2022.134791.
72. Mokoena S, Ganai M, Pathan T, Ike B, Obakachi V, Adu DK, Alake J, Kajee A, Shaik BB, Partap S. Design, synthesis, and biological evaluation of 1, 2, 4-triazolo [1, 5-a][1, 3, 5] triazine derivatives as E. coli DNA gyrase inhibitors. J Mol Struct. 2025;1336:141994. https://doi.org/10.1016/j.molstruc.2025.141994.
73. Obakachi VA, Kushwaha ND, Kushwaha B, Mahlalela MC, Shinde SR, Kehinde I, Karpoormath R. Design and synthesis of pyrazolone-based compounds as potent blockers of SARS-CoV-2 viral entry into the host cells. J Mol Struct. 2021;1241:130665. https://doi.org/10.1016/j.molstruc.2021.130665.
74. Adewumi AT, Mosebi S. Characteristic binding landscape of Estrogen receptor-α36 protein enhances promising cancer drug design. Biomolecules. 2023;13(12):1798. https://doi.org/10.3390/biom13121798.
75. Santos SJ, Valentini A. Brussonol and Komaroviquinone as inhibitors of the SARS-CoV-2 Omicron BA. 2 variant Spike protein: A molecular docking, molecular dynamics, and quantum biochemistry approach. J Mol Graphics Model. 2025;135:108914. https://doi.org/10.1016/j.jmgm.2024.108914.
76. Biernacki K, Ciupak O, Daśko M, Rachon J, Flis D, Budka J, Inkielewicz-Stępniak I, Czaja A, Rak J, Demkowicz S. Development of potent and effective SARS-CoV-2 main protease inhibitors based on maleimide analogs for the potential treatment of COVID-19. J Enzyme Inhib Med Chem. 2024;39(1):2290910. https://doi.org/10.1080/14756366.2023.2290910.

Publisher's note